

# Heliospheric Origin of Gamma-Ray Bursts

1

Ti-Pei Li

High Energy Astrophysics Laboratory, Institute of High Energy Physics

Academy of Sciences, P.O.Box 918, Beijing, China

Electronic mail: litp@ASTROSV1.IHEP.AC.CN

## Abstract

Systematic variations of average observational characteristics and correlation properties between different parameters of gamma-ray bursts (GRBs) with time from 1991 April to 1994 September are revealed. It is hard to explain the observed long-term variability by variations of experimental conditions. The variability of GRB properties with the time scale of months to years, together with the similarity between GRBs, solar hard X-ray flares and terrestrial gamma-ray flashes, may indicate an origin of GRBs, at least partly, within the heliosphere. Large-voltage and high-temperature pinch plasma columns produced by disruptive electrical discharges in the outer heliosphere can generate hard X-ray and  $\gamma$ -ray flashes with energy spectra and spectral evolution characters consistent with that observed in GRBs.

**Key Words:** Gamma-ray burst – Heliosphere – Solar wind

## 1. Introduction

GRBs are intense, brief flashes of non-thermal hard X-rays and  $\gamma$ -rays from random directions and at unpredictable times. GRBs have been extensively studied since their discovery (Klebesadel, Strong & Olson 1973). Several satellites were launched to observe the bursts and a large number and wide variety of models were put forwards to explain their origin. The Burst and Transient Source Experiment (BATSE) on board the *Compton Gamma Ray Observatory* (CGRO) was launched in April 1991. BATSE, with an unprecedented sensitivity,  $\sim 1 \times 10^{-7}$  erg cm $^{-2}$ , has revolutionized the study about the nature of these objects and raised more debates on it as well.

After more than twenty five years of the discovery of GRBs, their origin still remains a continuing puzzle. The most significant characteristic of these transient events is their complexity in morphology. The duration of GRB ranges from a few milliseconds to hundred of seconds and the temporal structure displays complicated patterns, of which basic features are still difficult to be summarized. In all timescales, some bursts have complex profiles, rich in fluctuating structures and some smooth, sometimes single structure profiles. None of the models suggested so far for GRBs can provide a satisfactory explanation to their main features in temporal and spectral characteristics.

The observed bursts are distributed isotropically on the sky, that exclude distant galactic disk populations from the GRB sources. The distributions of GRB intensities (peak counts  $C$  or peak flux  $P$ ), integral  $\lg N - \lg C$  or  $\lg N - \lg P$  diagrams, are consistent with the  $-3/2$  slope (expected

---

<sup>1</sup>submitted to *Astrophysics and Space Science*

for a homogeneous sample of monoluminosity in Euclidean space) for bright bursts, but considerably absent for bursts at low intensities. The incompatibility of the intensity distribution with a uniform distribution throughout space rules out local galactic disk sources. The only place left for GRBs at the Galaxy is at an extended galactic halo with distances  $d \approx 50 - 100$  kpc (Hartmann 1994). The intensity distribution is widely accepted as a strong support to an extragalactic origin that the deviation from the  $-3/2$  power law is due to cosmological effects (Mao & Paczyński 1992; Piran 1992; Dermer 1992). The debate on the distance scale to GRBs is now mainly between the galactic halo and cosmological distances (eg. Lamb 1995; Paczyński 1995).

Some average properties of GRBs detected by BATSE, e.g. duration and spectral hardness, show systematic variations with time from 1991 April to 1994 September (Li 1996). These variations are difficult to be explained with experimental effects. The analysis procedures and more results on the variability of properties of correlation between different GRB parameters are presented in section 2 of this paper in detail. The existence of GRB long-term variability with a time scale of months to years indicates a heliospheric origin. In section 3 a model of GRBs originating from disruptive discharges in instable plasma of the outer heliosphere is described. A study of two kinds of  $\gamma$ -ray flashes, solar flares and terrestrial  $\gamma$ -ray flashes, which were also detected by BATSE and certainly originated within the heliosphere, is made in comparison with GRBs in section 4.

## 2. Long-term variability

BATSE, having been continually detecting GRBs at a rate of about one event per day since April 1991, makes it possible to study long-term variability of GRB observational properties. The third BATSE (3B) Catalog of gamma-ray burst (Meegan *et al.* 1996) consists of 1122  $\gamma$ -ray burst triggers and covered the time interval from 1991 April 21 until 1994 September 19. To check through the 3B catalog to see if there exists systematic change with time in values of a burst parameter, we divided the observation time (TJD from 8367 to 9614, where the truncated Julian Date TJD=JD-2440000.5) into a few epoch periods with the same length and calculated the average value of the parameter for each period.

### 2.1 Duration and hardness

The parameter  $T_{90}$  is used to measure the duration of a burst.  $T_{90}$  is the time interval in which the integrated counts from the burst increases from 5% to 95% of the total observed counts. Firstly we calculated the average  $\bar{T}$  and standard deviation  $\sigma_T$  of all the values of  $T_{90}$  listed in the 3B catalog, and then divided the observation time into four periods and for each of the four periods calculated the average,  $\langle T_{90} \rangle$ , from all the  $n$  bursts in each period for which  $T_{90}$  are available. The result is shown in Fig.1(a). The statistical error of  $\langle T_{90} \rangle$  is estimated by  $\sigma_T/\sqrt{n}$ . One can see from Fig.1(a) that  $\langle T_{90} \rangle$  evidently decreases with time, from  $41.4 \pm 3.6$  s during 91.4 – 92.2 to only  $25.0 \pm 3.4$  s during 93.11 – 94.9, at a rate, relative to  $\bar{T}$ , of  $(-18.3 \pm 5.6)\% \text{ yr}^{-1}$ , which was derived by a weighted linear least-squares fit with a reduced  $\chi^2 = 0.21$  (the reduced  $\chi^2$  is the fitting  $\chi^2$  over the degrees of freedom). The linear regression has  $3.3\sigma$  significance for the null hypothesis that  $T_{90}$  and observation time are uncorrelated.

The variability of  $T_{90}$  has also been studied by the correlation analysis without binning. The correlation coefficient for a sample of  $n$  pairs of  $x, y$  values is defined as

$$r(x, y) = \frac{\sum_{i=1}^n \nu(i)}{\sqrt{\sum (x - \bar{x})^2 \sum (y - \bar{y})^2}}$$

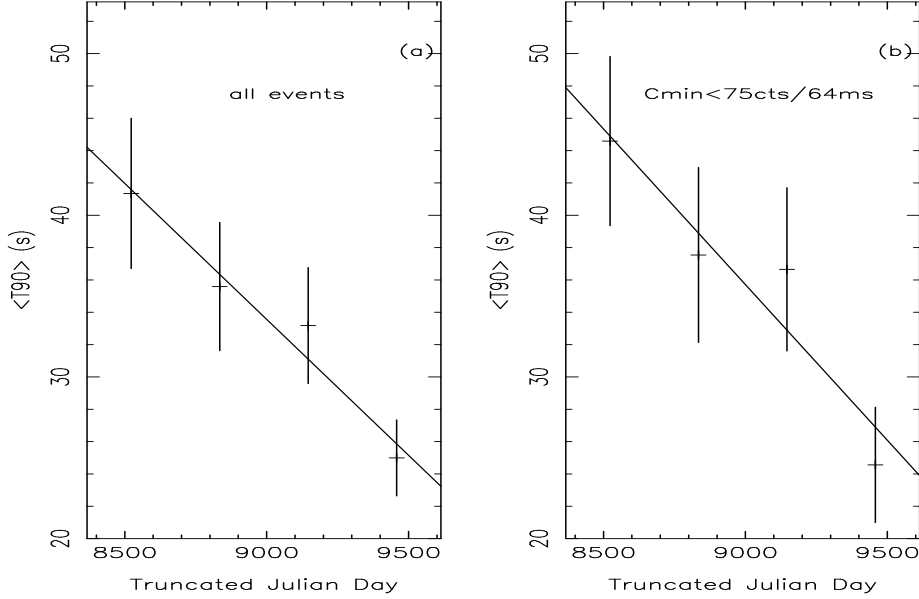


Figure 1: Average burst duration  $\langle T_{90} \rangle$  against observation time of 3B bursts. (a) For all the bursts for which  $T_{90}$  are available in 3B catalog; (b) For bursts in 3B catalog with trigger thresholds  $C_{min} < 75$  cts on the 64 ms timescale.

where  $\nu(i) = (x(i) - \bar{x})(y(i) - \bar{y})$ . For the total  $n = 834$  bursts in 3B catalog for which  $T_{90}$  are available, the value of the correlation coefficient between  $T_{90}$  and the observation date  $t$  was calculated as  $r(T_{90}, t) = -0.12$ . The significance of a value of  $r$  to test the hypothesis that  $T_{90}$  and  $t$  are uncorrelated can be evaluated by the statistic  $u = r\sqrt{(n-2)/(1-r^2)}$  which satisfies a Student's  $t$ -distribution with  $n-2$  degrees of freedom under the null hypothesis (Siegel 1956). We found  $u = -3.4$ . As  $n = 834 \gg 1$ , the statistic  $u$  here follows the standard normal distribution,  $u = -3.4$  indicates a result with  $3.4\sigma$  significance, which is consistent with the result from regression analysis ( $3.3\sigma$ ) and the probability that the observed variability of  $T_{90}$  comes from the statistical fluctuation is less than  $3.2 \times 10^{-4}$ .

In the 3B catalog four energy fluences  $F_1, F_2, F_3$  and  $F_4$ , in units of  $\text{erg cm}^{-2}$  and covering the energy ranges 20-50, 50-100, 100-300 keV and  $E > 300$  keV respectively, are given for 867 bursts. The average fluences of bursts in each of four periods were calculated for the four energy channels separately and shown in Fig.2(a). The fitted change slopes from Fig.2(a) are listed in Table 1. One can see from Fig.2(a) and Table 1 a steady trend that the average fluence increases quicker for higher energy channel.

Table 1: Change rates of average fluences

Energy range (keV)	20 – 50	50 – 100	100 – 300	> 300
Change rate (% yr <sup>-1</sup> )	$10.2 \pm 10.2$	$6.2 \pm 7.3$	$17.8 \pm 9.7$	$29.0 \pm 15.8$

The ratio  $H_{24} = F_2/F_4$  is used to measure spectral hardness. In statistics of  $H_{24}$  a few events with very small  $F_4$  seriously influence the average and disturb the general trend of variability much. Only three isolated bursts in total 690 bursts with  $F_4 > 0$  have  $H_{24} > 40$ , we picked them out and calculated  $\langle H_{24} \rangle$  and its standard deviation for residual 687 events for each period. The results shown in Fig.2(b) reveal that the energy spectra of GRBs in 3B catalog became harder with time ( $\langle H_{24} \rangle$  decreased, from  $1.15 \pm 0.17$  during 91.4 – 92.2 to only  $0.44 \pm 0.18$  during 93.11 – 94.9, at a rate of  $(-35.1 \pm 11.9)\% \text{ yr}^{-1}$ ).

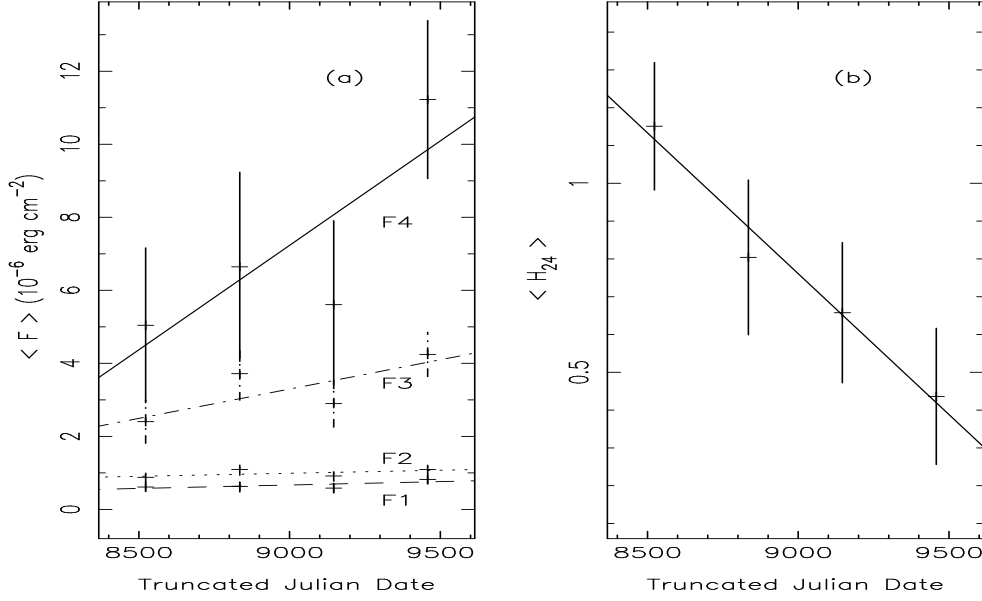


Figure 2: Evolution of burst spectral property. (a) Average energy fluences against observation time for 3B bursts.  $F_1, F_2, F_3$  and  $F_4$  are fluences covering the energy ranges 20-50, 50-100, 100-300 keV and  $E > 300$  keV respectively; (b) Average spectral hardness ratio against observation time for 3B bursts. The hardness ratio  $H_{24} = F_2/F_4$ , from all the bursts for which  $F_2$  and  $F_4$  are available and  $F_2/F_4 < 40$ .

## 2.2 Experimental effects

Since March of 1992 there are gaps in the data of GRB intensity, fluence or duration due to the errors of CGRO tape recorders, the problem has significantly reduced since March of 1993 (Meegan *et al.* 1996). The number  $n$  of events for which  $T_{90}$  can be measured and that of total detected GRBs,  $N$ , for each period, are listed in Table 2. A less value of the ratio  $n/N$  reflects greater effect of data gaps. As the change behaviour of  $\langle T_{90} \rangle$  and  $\langle H_{24} \rangle$ , shown in Fig.1(a) and Fig.2(b), is quite different with that of  $n/N$ , shown in Fig.3(a), it is hard to interpret the systematic variations of duration and hardness ratio by the effect of data gaps.

The observed variation of burst duration can not be explained by the variation of background either. The average of trigger thresholds  $C_{min}$  on the 64 ms timescale, set by command to a  $5.5\sigma$  deviation above background, was calculated for each period and also listed in Table 2 and shown in Fig.3(b). The values of  $\langle C_{min} \rangle$  have not shown a systematic change with time.

Table 2: Statistics of 3B bursts in four periods

Period (yy.mm.dd)	Number of Bursts			$\langle C_{min} \rangle$ (cts/64ms)	$\langle T_{90} \rangle$ (s)	$\langle H_{24} \rangle$
	$n$	$N$	$n/N$			
91.04.21–92.02.27	216	249	0.87	$69.9 \pm 1.5$	$41.4 \pm 3.6$	$1.15 \pm 0.17$
92.02.28–93.01.04	168	271	0.62	$70.6 \pm 3.5$	$35.6 \pm 4.1$	$0.80 \pm 0.21$
93.01.05–93.11.12	208	297	0.70	$66.7 \pm 0.9$	$33.2 \pm 3.7$	$0.66 \pm 0.19$
93.11.13–94.09.19	242	305	0.79	$72.7 \pm 2.6$	$25.0 \pm 3.4$	$0.44 \pm 0.18$

For further inspecting the effect of background variation on  $\langle T_{90} \rangle$ , the  $C_{min}$  distribution for bursts in the 3B catalog was made and shown in Fig.4(a). Most values of  $C_{min}$  are smaller than 75 cts/64ms. The bursts were grouped into four subsets with  $C_{min} < 65$ ,  $65 \leq C_{min} < 68$ ,  $68 \leq C_{min} < 75$

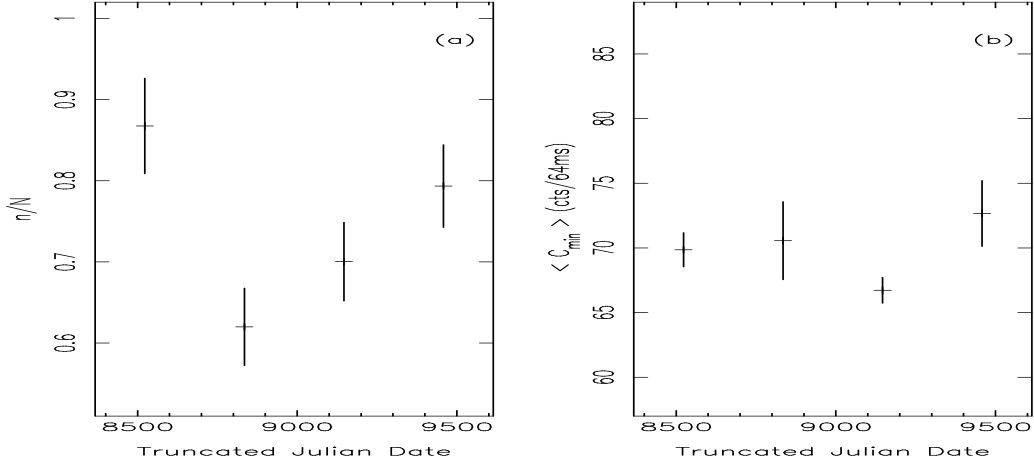


Figure 3: Variations of BATSE data gaps and backgrounds. (a) Efficiency ratio  $n/N$  for measurement of  $T_{90}$  against observation time, where  $N$  is the total number of detected bursts during a period and  $n$  the number of bursts for which  $T_{90}$  can be measured during the same period. (b) Average trigger threshold on the 64 ms timescale against observation time.

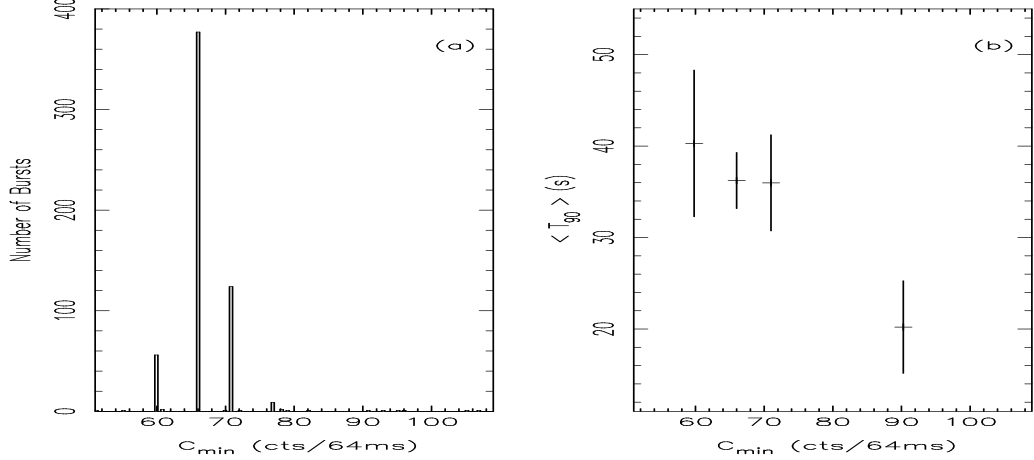


Figure 4: Distribution of trigger thresholds on the 64 ms time scale of 3B catalog; (b) Correlation between duration and trigger threshold of 3B bursts.

and  $C_{min} \geq 75$  (in units of cts/64ms) respectively. The average values of  $T_{90}$  for each subsets were calculated and shown in Fig.4(b). There is no visible dependence between  $\langle T_{90} \rangle$  and  $C_{min}$  except such detected bursts under highest trigger thresholds of  $C_{min} \geq 75$  cts/64ms. Fig.1(b) shows that the average duration  $\langle T_{90} \rangle$  for bursts having  $C_{min} < 75$  cts/64ms also decreases with time at a rate of  $(-17.1 \pm 5.2)\% \text{ yr}^{-1}$ , consistent with that derived from all bursts. Therefore, the observed duration variability can not be interpreted with background variation.

Another experimental condition with secular change is spacecraft altitude. Fig.5 shows CGRO altitude history. After comparing Fig.5 with Fig.1 and Fig.2, one can see that the observed long-term variations of duration and hardness can not be due to the altitude variation either.

There exists a positive dependence of burst fluences against their durations. Fig.6(a) shows the correlation of  $\lg F$  and  $\lg \langle T_{90} \rangle$  in 3B events where the regression line has a slope of  $\lambda = 0.52 \pm 0.02$ . If the decrease of average duration is caused by decrease of detection efficiency for longer events by some unknown reasons, a decrease of average fluence with time should be expected. But the measured results for fluences show an opposite trend, see Fig.6(b), indicating that the detected changes should be intrinsic.

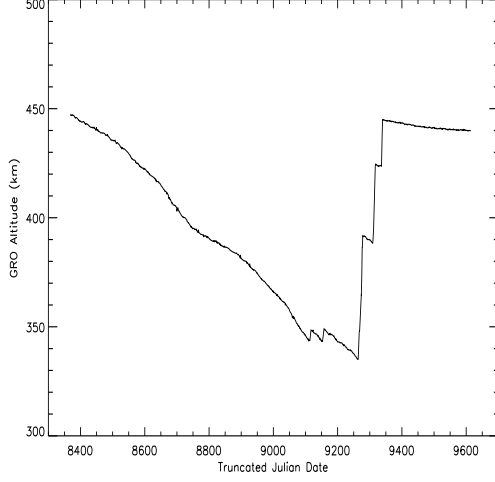


Figure 5: CGRO altitude vs. time.

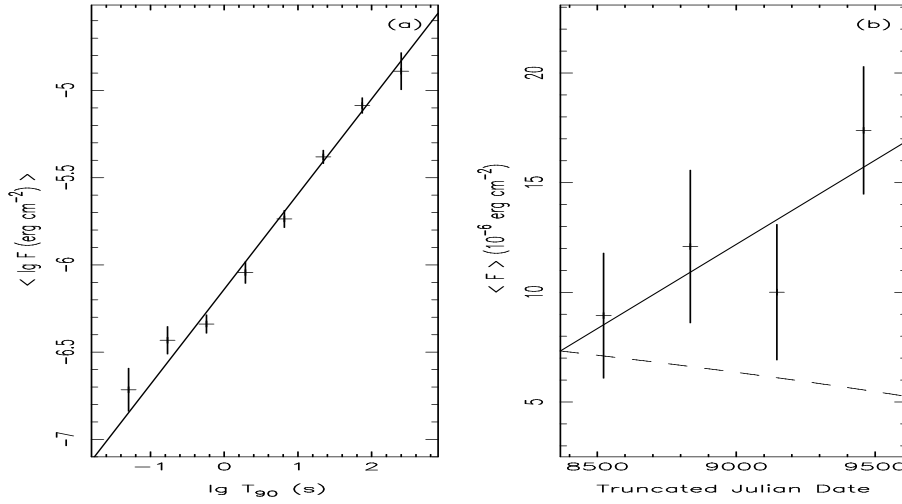


Figure 6: (a) Correlation between fluence and duration of 3B bursts; (b) Average fluence against observation time, solid lines represent the measured results and dashed line is the expectation calculated from the regression line for  $\langle T_{90} \rangle$  in Fig.1(a) and correlation between  $F$  and  $T_{90}$  and normalized at TJD=8367.

### 2.3 Correlation properties

The relationship between two parameters of GRBs reflects the nature of GRB production process. Long-term variability also found for different correlation property of GRBs in 3B catalog, which is more difficult to be interpreted with experimental effects (Li 1997). There are total 807 bursts in the 3B catalog for which both  $F$  and  $T_{90}$  are available. Calculating the correlation coefficient between  $\lg F$  and  $\lg T_{90}$  for the 807 bursts we get  $r(\lg F, \lg T_{90}) = 0.67 \pm 0.02$ . The statistical error of the correlation coefficient is estimated by the bootstrap technique (Efron 1979; Diaconis & Efron 1983). To check through the 3B catalog to see if there exists systematic change with time in the relationship between  $F$  and  $T_{90}$ , we divide the observation time  $t$  (TJD from 8367 to 9614 for 3B catalog) into five epoch periods, letting each period has nearly equal number of bursts for which both  $F$  and  $T_{90}$  are available, and calculate the correlation coefficient  $r(\lg F, \lg T_{90})$  and its statistical error for each period. Fig.7(a) shows the result. From Fig.7(a) one can see that the correlation coefficient  $r(\lg F, \lg T_{90})$  increased from  $0.60 \pm 0.04$  during 91.111 – 91.329 to  $0.71 \pm 0.03$  during 94.154 – 94.262 at a rate  $\lambda(r, t) = 0.038 \pm 0.017 \text{ yr}^{-1}$ , which was derived by a weighted linear least-squares fit. The linear increasing of correlation coefficient  $r(\lg F, \lg T_{90})$  with observation time  $t$  has  $2.2\sigma$  significance for the null hypothesis that  $r(\lg F, \lg T_{90})$  and observation time  $t$  are uncorrelated.

Now we study the variability of correlation coefficient between spectral hardness and duration. The ratio  $H_{32} = F_3/F_2$  is used to measure spectral hardness. As events with very small  $F_2$  considerably disturb the general trend of variability of  $H_{32}$ , we pick a couple of events with  $H_{32} > 10$  out in the statistics through this work. There is a general trend of hardness with short events being harder (Dezalay *et al.* 1992; Kouveliotou *et al.* 1993a), but the variation behaviour of hardness against duration for short bursts is quite different with that for long bursts: the correlation coefficient  $r(H_{32}, \lg T_{90})$  between  $H_{32}$  and  $\lg T_{90}$  for 583 long bursts with  $T_{90} > 2$  s in the 3B catalog is 0.01 and that for 178 short bursts with  $T_{90} < 2$  s is  $-0.11$ . No visible change of the correlation coefficient between  $H_{32}$  and  $\lg T_{90}$  with time has been found for long bursts, the slope of the regression line of  $r(H_{32}, \lg T_{90})$  on  $t$  fitted to the values of five epochs being  $0.005 \pm 0.039 \text{ yr}^{-1}$ , whereas evident variation existed in short bursts, shown in Fig.7(b). The correlation coefficient  $r(H_{32}, \lg T_{90})$  for bursts with  $T_{90} < 2$  s increased from  $-0.52 \pm 0.11$  during 91.111 – 91.324 to  $0.16 \pm 0.13$  during 94.43 – 94.262. The regression line in Fig.7(b) has a slope of  $0.239 \pm 0.057 \text{ yr}^{-1}$ , showing a  $4.2\sigma$  long-term variability.

### 2.4 Bimodality

The bursts duration distribution can be divided to two sub-groups according to  $T_{90}$ : Long bursts with  $T_{90} > 2$  s and short bursts with  $T_{90} < 2$  s (Kouveliotou *et al.* 1993b; Meegan *et al.* 1996). We found that the variability behaviour of observed GRB parameters is also bimodal: duration becoming shorter and spectrum harder is only observed for long bursts in the 3B catalog, but not for short ones. On the other hand, the variability of correlation properties between different parameters, e.g.  $F$  and  $T_{90}$ , or  $H_{32}$  and  $T_{90}$ , is revealed in short bursts more obviously than that in long bursts. Fig.8 show time variation behaviour of the parameters (duration, hardness ratio and fluence), and the correlation coefficients between fluence and duration and between hardness and duration for long bursts and for short bursts in the 3B bursts separately. The change slopes derived by the linear fitting procedure are listed in Table 4. For short bursts both  $r(\lg F, \lg T_{90})$  and  $r(H_{32}, \lg T_{90})$  increased with time evidently with  $4\sigma$  significance, but for long bursts the change rate of  $r(\lg F, \lg T_{90})$  was only one third of that for short bursts and no visible change found for  $r(H_{32}, \lg T_{90})$ .

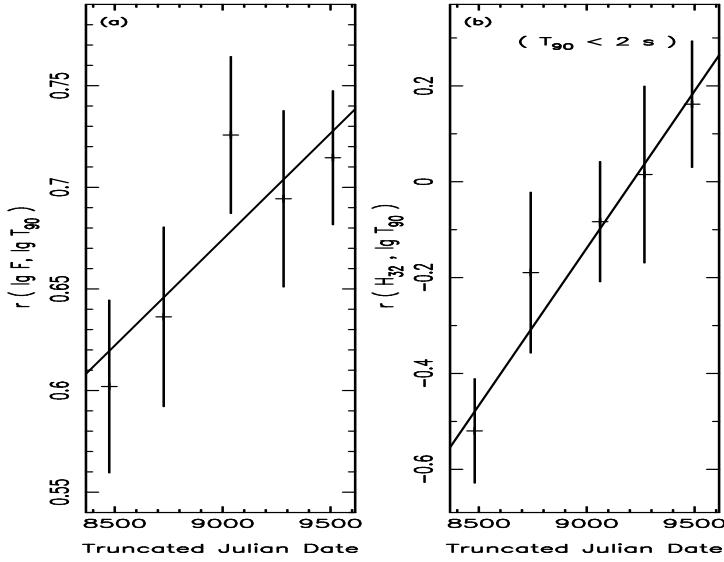


Figure 7: Evolution of correlation coefficients. (a) Correlation coefficient between  $\lg F$  and  $\lg T_{90}$  against observation time for 3B bursts. (b) Correlation coefficient between hardness ratio  $H_{32}$  and  $\lg T_{90}$  against observation time for short 3B bursts with  $T_{90} < 2$  s.

Table 3: Change slopes of GRB properties

Property	Change slope ( $\text{yr}^{-1}$ )	
	short bursts ( $T_{90} < 2$ s)	long bursts ( $T_{90} > 2$ s)
$T_{90}$	$(-2.5 \pm 5.8)\%$	$(-15.7 \pm 5.0)\%$
$H_{24}$	$(12.0 \pm 27.2)\%$	$(-32.3 \pm 12.9)\%$
$F$	$(16.3 \pm 14.6)\%$	$(19.7 \pm 13.2)\%$
$r(\lg F, \lg T_{90})$	$0.20 \pm 0.05$	$0.064 \pm 0.028$
$r(H_{32}, \lg T_{90})$	$0.24 \pm 0.06$	$0.005 \pm 0.039$

## 2.5 Short bursts

From Fig.8(i) and (j) and Table 3 one can see that long-term variability of the correlation coefficient  $r(H_{32}, \lg T_{90})$  only show in short bursts with  $T_{90} < 2$  s, none in long bursts. Now we further inspect the correlation properties of short bursts.

There are 745 events in the 3B catalog for which both  $T_{90}$  and  $F$  are available. To show the relationship between hardness and duration, we divide the range  $0 - 200$  s of  $T_{90}$  into 22 bins, letting each bin includes nearly equal number of events, and calculate the average of  $T_{90}$ , average of  $H_{32}$  and their standard deviations for each bin. Fig.9 shows the result. It is noticeable in Fig.9 that a turn in the correlation behaviour between  $H_{32}$  and  $T_{90}$  occurs at  $T_{90} \simeq 0.55$  s as well as at 2 s. From Figure 10 (a) and (b), which show the  $H_{32} - \lg T_{90}$  distribution of 373 bursts during observation epoch  $t$  between 8367 and 9037 TJD and that between 9038 and 9614 TJD separately, one can see that the correlation behaviour between  $H_{32}$  and  $T_{90}$  of the brief bursts ( $T_{90} < 0.55$  s) is evidently changed with time.

Similar phenomena can also be found in the correlations between  $H_{41}$  and  $T_{90}$  and that between the peak flux  $P_{64}$ , the maximum flux in  $50 - 300$  keV ( $\text{ph. cm}^{-2}\text{s}^{-1}$ ) integrated over 64 ms timescale, and  $T_{90}$  for the short bursts. The correlation coefficient  $r(H_{41}, \lg T_{90})$  evidently increased with observation time at a rate  $\lambda = 0.36 \pm 0.08 \text{ yr}^{-1}$  for the brief bursts shown in Fig.11(a), but no visible variation is found in Fig.11(b) for the medium bursts ( $\lambda = 0.008 \pm 0.12 \text{ yr}^{-1}$ ). For the brief bursts the correlation coefficient of  $r(P_{64}, \lg T_{90})$  is positively correlated with the observation time (the slope of regression



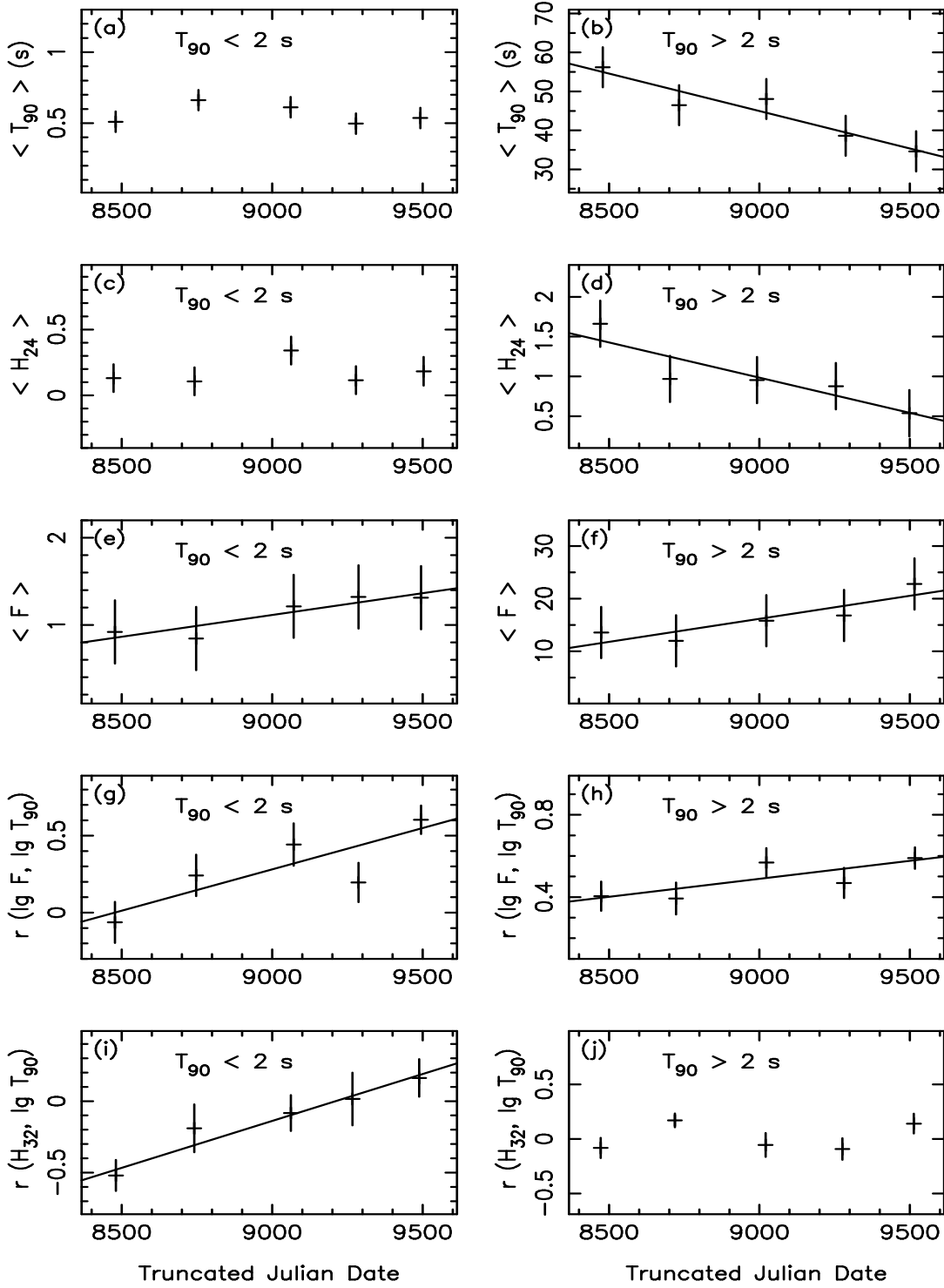


Figure 8: Evolution of average values of parameters  $T_{90}$ ,  $H_{24}$ ,  $F$  and correlation coefficients  $r(\lg F, \lg T_{90})$ ,  $r(H_{32}, \lg T_{90})$  for two types of GRBs in the 3B catalog. (a),(c),(e),(g),(i) for bursts with  $T_{90} < 2$  s, (b),(d),(f),(h),(j) for bursts with  $T_{90} > 2$  s.  $H_{24} = F_2/F_4$  and  $H_{32} = F_3/F_2$ . A couple of bursts with  $H_{24} > 40$  were excluded from the statistics in (c) and (d), and that with  $H_{32} > 10$  in (i) and (j).

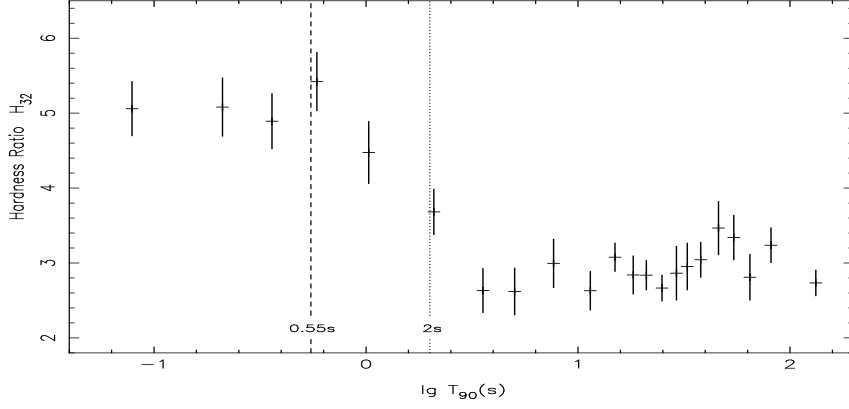


Figure 9: Distribution of  $H_{32} - \lg T_{90}$  for all the events in 3B catalog during the period between 8367 and 9614 TJD.

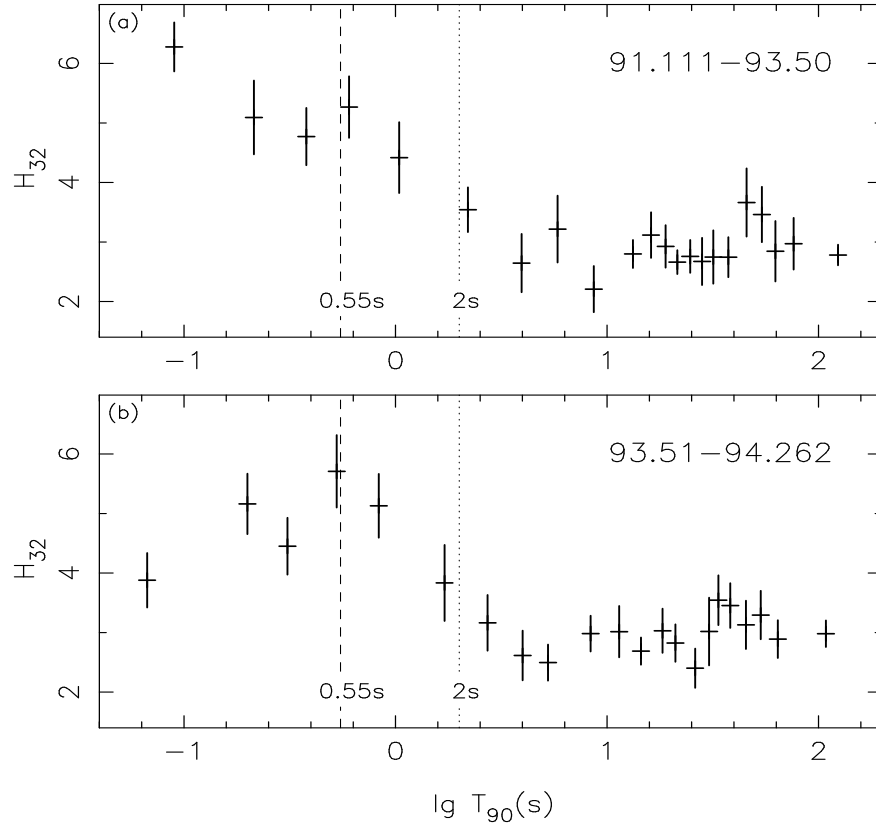


Figure 10:  $H_{32} - \lg T_{90}$  distributions. (a) For bursts during the period between 8367 and 9037 TJD. (b) For bursts during the period between 9038 and 9614 TJD.

line  $\lambda = 0.26 \pm 0.06 \text{ yr}^{-1}$  in Fig.11(c)), but for the medium bursts a negative correlation between  $r(P_{64}, \lg T_{90})$  and the observation time appears with  $\lambda = -0.15 \pm 0.10 \text{ yr}^{-1}$  shown in Fig.11(d).

To get a free of binning estimation of the significance level for the time variability of the correlation between  $x$  and  $y$  from a sample of  $n$  points  $(x, y, t)$ , the equation of the line of regression of  $x$  on  $t$ ,  $x = A_x + B_x t$ , and that of  $y$  on  $t$ ,  $y = A_y + B_y t$ , are firstly derived by the method of least squares. For each burst  $i$  ( $i = 1, \dots, n$ ) with parameters  $(x(i), y(i), t(i))$  the following quantity  $\nu(i) = (x(i) - x_0(i))(y(i) - y_0(i))$  with  $x_0(i) = A_x + B_x t(i)$  and  $y_0(i) = A_y + B_y t(i)$  is calculated. The correlation coefficient between  $\nu$  and  $t$ ,  $r(\nu, t)$ , for the sample of  $n$  pairs of  $\nu, t$ -values now can be calculated, the standard deviation of the derived  $r(\nu, t)$  can be evaluated by the bootstrap technique and the relative portion  $\xi$  of the correlation coefficient less or equal to 0 (or greater or equal to 0 if  $r(\nu, t) < 0$ ) among the bootstrap samples can be taken as an estimate of the significance level. The obtained values of  $r(\nu, t)$  of the parameter pairs  $(H_{32}, \lg T_{90})$ ,  $(H_{41}, \lg T_{90})$ , and  $(P_{64}, \lg T_{90})$  are listed in Table 4 for the two types of burst separately, where the standard deviations and significance levels are derived from  $10^7$  bootstrap samples for each case.

Table 4: Significance levels  $\xi$  of correlation variations

Correlated Parameters (x, y)	$T_{90} < 0.55\text{s}$		$0.55\text{s} < T_{90} < 2\text{s}$	
	$r(\nu, t)$	$\xi$	$r(\nu, t)$	$\xi$
$H_{32}, \lg T_{90}$	$0.30 \pm 0.09$	$2.1 \times 10^{-4}$	$-0.03 \pm 0.10$	0.38
$H_{41}, \lg T_{90}$	$0.39 \pm 0.07$	$9.3 \times 10^{-5}$	$-0.07 \pm 0.11$	0.26
$P_{64}, \lg T_{90}$	$0.36 \pm 0.07$	$4.8 \times 10^{-6}$	$-0.16 \pm 0.09$	$4.1 \times 10^{-2}$

One can see that the three correlation coefficients listed in Table 4 have quite different variation behaviour between the two types of burst and significant (near to or great than  $4\sigma$ ) variations appear in the correlation properties of the brief bursts ( $T_{90} < 0.55 \text{ s}$ ).

### 3. A discharge model

Alfvén (1981) has stressed the importance of studying electric current circuits in plasmas to understanding phenomena occurred in the magnetosphere till galactic dimensions, and held that many of the explosive events observed in cosmic physics are produced by exploding electric double layers. In a circuit with inductance  $L$  and current  $I$  in plasma, electric double layers can be produced, in which large potential drops may be built up over distances of the order of some tens of the Debye lengths. A disruption of the current in a layer by plasma instability will cause an explosion: the layer voltage,  $V = L(dI/dt)$ , may exceed the normal value by several orders of magnitude and the magnetic energy stored in the circuit being suddenly released in the layer, will cause the plasma column to collapse to a much smaller radius by inward magnetic pressure of the discharging current (Z pinch) (Krall & Trivelpiece 1973) and the resulting compressed, large-voltage and high-temperature discharge column will radiate energetic photons from the inverse Compton scattering between the high-energy electrons and thermal photons. In an isotropic thermal emission with mean photon energy  $\bar{h\nu}$ , the mean energy of a scattered photon from an electron with an energy  $\epsilon$  is  $\bar{E} = \frac{4}{3}(\frac{\epsilon}{mc^2})^2 \bar{h\nu}$  (Ginzburg & Syrovatskii 1964). Let the temperature of a pinch discharge column is  $T$  (K), the differential photon density of the thermal emission at frequency  $\nu$  is  $n_\nu(T) = B_\nu(T)[1 - \exp(-\tau(\nu))]$ , where  $B_\nu(T)$  is the photon density of a black body and the optical depth

$$\tau(\nu) = 4.1 \times 10^{-23} T^{-3.5} \left(\frac{h\nu}{kT}\right)^{-3} (1 - e^{-\frac{h\nu}{kT}}) \bar{g} \int N^2 dl$$

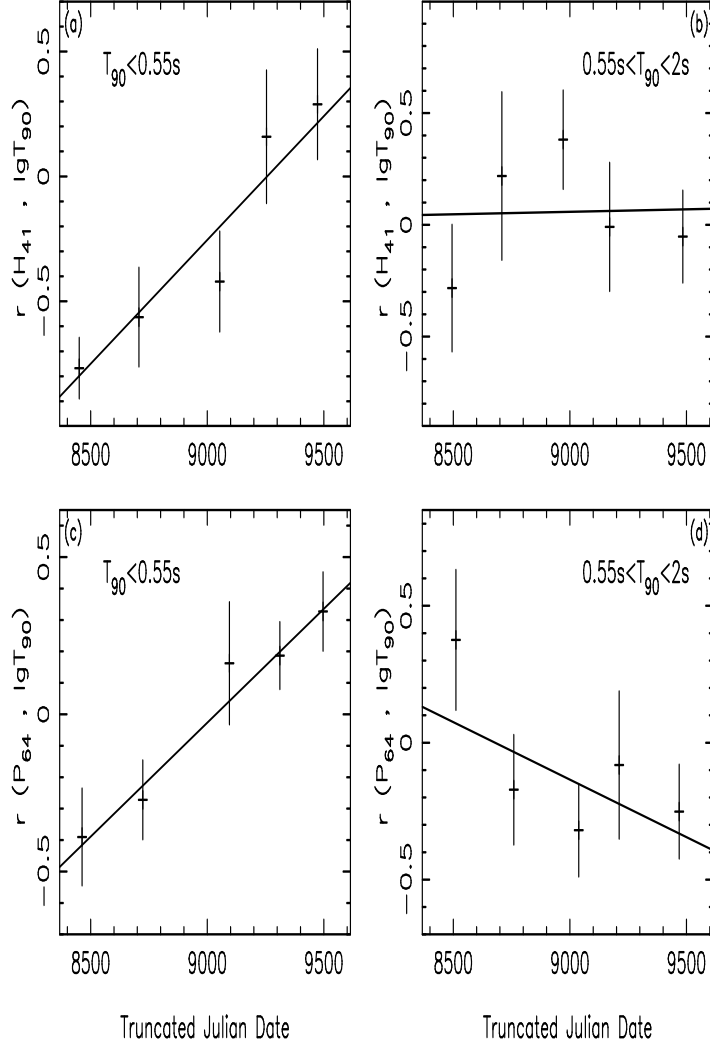


Figure 11: Correlation coefficient vs. observation time. For each figure the observation time period of 3B catalog is divided into five epoch periods by letting each period has nearly equal number of available events. The correlation coefficient  $r$  is calculated for each bin and its standard deviation is estimated by the bootstrap technique. A couple of isolated events with relevant parameter  $H_{41} > 150$  or  $P_{64} > 15$  are excluded from statistics. (a)  $r(H_{41}, \lg T_{90})$  vs. observation epoch for  $T_{90} < 0.55s$ . (b)  $r(H_{41}, \lg T_{90})$  vs. observation epoch for  $0.55s < T_{90} < 2s$ . (c)  $r(P_{64}, \lg T_{90})$  vs. observation epoch for  $T_{90} < 0.55s$ . (d)  $r(P_{64}, \lg T_{90})$  vs. observation epoch for  $0.55s < T_{90} < 2s$ .

with the emission measure  $\int N^2 dl$  being in  $\text{cm}^{-5}$  and average Gaunt factor  $\bar{g}$  taken as the approximation (Kulsrud 1954)

$$\bar{g} = \frac{\sqrt{3}}{\pi} \ln \frac{\sqrt{0.76 + h\nu/kT} + 0.87}{\sqrt{0.76 + h\nu/kT} - 0.87}$$

For thermal emissions of temperature  $T = 10^6$  K and optical depth  $\tau_0 = 0.1$  at  $h\nu = 1kT$ , the mean photon energy  $\sim 72$  eV, then the mean energy of a scattered photon from an electron with  $\epsilon = 100$  MeV can be calculated as  $\sim 3.7 \times 10^3$  keV. Therefore, the large voltage and high temperature discharge column is an effective radiator of hard X-rays and soft  $\gamma$ -rays.

The existence of any intrinsic variability of GRB properties with a time scale of months to years can not be interpreted with either the galactic or cosmological origin. Only the decrease in solar activity during the 3B observation period remains to be a reason, and thus GRBs, or at least a part, should be originated within the effective region of the solar wind. GRBs may be possible from exploding electric double layers in instable plasma within the heliosphere (Li 1996). With respect to their isotropic spatial distribution, GRBs should be produced far away from the Sun. A distance of about 100 AU can satisfy the constraint from observed GRB isotropy distribution (the measured dipole moment  $\cos \theta \sim 0.01$ ) and that from triangulation and direct positioning for a few bursts. At the solar-wind terminal shock, near the heliospheric boundary and surrounding the solar system, lies an abrupt discontinuity, turbulent and complex structure (Suess 1990), at which various intriguing phenomena may occur, GRB might be one of them. The typical energy released in a GRB produced at a distance of 100 AU is about  $10^{26} f$  ergs, where  $f$  is the beaming solid angle fraction. If emission is beamed into an angular region of  $\sim 1$  deg<sup>2</sup>, the typical energy of GRBs will be only  $\sim 2 \times 10^{21}$  ergs, equivalent just an average thunderstorm (Battan 1961).

A burst with total released energy  $2 \times 10^{21}$  erg emits  $\sim 2 \times 10^{28}$  photons (60 keV/ph assumed). If each discharge electron produces one burst photon through the inverse Compton scattering with thermal photons, a discharging current of  $\sim 2 \times 10^8$  A can produce the burst emission with a 10 s duration. A current flowing in the heliospheric plasma may contract by the magnetic confinement and form a plasma cable with much larger density than the surroundings (Alfvén 1981). In the disruptive discharge the cable is further pinched into a very narrow column. The interaction length of the Compton scattering between energetic electrons and thermal photons in a plasma column with diameter  $d = 1$  m and temperature  $10^6$  K, which is pinched from a initial current cable with diameter  $d_0 = 0.1$  AU =  $1.5 \times 10^{12}$  cm and density  $N_0 = 1$  cm<sup>-3</sup>, is only  $\sim 10$  km. The density of the pinch column can be estimated as  $N \sim 2 \times 10^{20}$  cm<sup>-3</sup> and optical depth  $\tau_0 \sim 0.1$ .

The GRB spectra accumulated by the Spectroscopy Detectors (SD) of BATSE are described well by the following empirical Band *et al.* (1993) model

$$\begin{aligned} N(E) &= A\epsilon^\alpha \exp(-E/E_0) & (\alpha - \beta)E_0 &\geq E \\ &= A[(\alpha - \beta)E_0]^{\alpha - \beta} \exp(\beta - \alpha)E^\beta & (\alpha - \beta)E_0 &\leq E \end{aligned}$$

with  $\alpha \sim -1, \beta \sim -2$ . The peak power energy  $E_{pk} = (2 + \alpha)E_0$ . Our calculations show that  $\gamma$ -ray flashes produced by large voltage and high temperature discharge plasma columns can also be described well by this model (Li & Wu 1997). We assumed a simple discharge model that an initial discharge voltage  $V_0$  is produced at time  $t = 0$ , the discharging current firstly has a Gaussian rise,  $i(t) \propto \exp(-(\frac{t_m - t}{a_1})^2)$  till to its maximum at  $t = t_m$  and then falls exponentially with a decay constant  $a$ ,  $i(t) \propto \exp(-\frac{t - t_m}{a})$ ; the potential difference falls proportionally to the total quantity of charge transferred by the current,  $V(t) = V_0 - B \int_0^t i(t) dt$ . At time  $t$ , the kinematic energy of a discharge electron increases lineally along the path from 0 at the cathode to  $V(t)$  at the anode, the

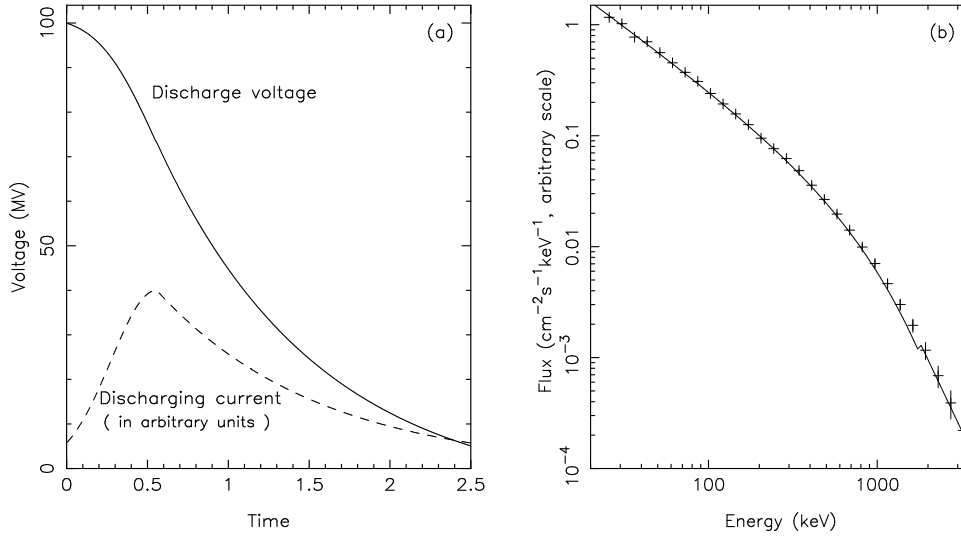


Figure 12: An example of discharge model. (a) Time histories of discharge voltage (solid line) and current (dashed line), the voltage is in units of  $10^6$  V, current in arbitrary units, time is scaled by the exponential decay constant of the current. (b) The calculated time-averaged spectrum (crosses) from a discharge column with temperature  $T = 1 \times 10^6$  K, optical depth at  $1kT$   $\tau_0 = 0.1$  and time histories of voltage and current shown in (a), observed over a scattering angle interval  $0^\circ - 0.5^\circ$ . The flux is in arbitrary scale. The solid line shows the Band *et al.* spectrum with parameters  $\alpha = -1.12$ ,  $\beta = -2.28$  and  $E_{pk} = 826.4$  keV.

observed radiation is a summation of the scattered photons from electrons with kinematic energies between 0 and  $V(t)$ . For example, let  $V_0 = 100$  MV,  $a_1 = 0.4a$ , total discharge time  $D = 2.5a$ , the voltage at the end of discharge  $V_D = 5$  MV, the corresponding time histories of discharge voltage and current are shown in Fig.12(a), where the time is scaled by the current decay constant  $a$ . Differential scattered photon spectra from electrons with different energies and isotropic thermal emission with  $T = 10^6$  K and  $\tau_0 = 0.1$  were calculated by the Klein-Nishina formula. Because the plasma instability, the discharge column may be twisting, flickering and branching, an observed spectrum should be an average over a certain interval of scattering angle. As an example, the crosses in Fig.12(b) show the expected spectrum observed by SD of BATSE for scattered photons with scattering angle  $\leq 0.5^\circ$ , the error bars were estimated by assuming the total number of recorded photons of  $E \geq 20$  keV being  $2 \times 10^4$ , a  $E^{-2}$  background spectrum with a flux of  $1 \times 10^{-2} \text{ cm}^{-2} \text{ s}^{-1} \text{ keV}^{-1}$  at 100 keV and in considering the SD full-energy peak efficiency (Fishman *et al.* 1989). Fitting the Band *et al.* model to the simulated spectrum in the region of  $E \geq 20$  keV we got the solid line in Fig.12(b) with  $\alpha = -1.1$ ,  $\beta = -3.2$ ,  $E_{pk} = 748.0$  keV and the reduced  $\chi^2 = 0.59$ , showing the discharge model can produce a typical GRB spectrum.

Producing Band *et al.* spectra is a general property of the discharge mechanism. We calculated 100 spectra with different values of the discharge model parameters. In our calculations, the initial voltage  $V_0$  was sampled uniformly from the region of  $50 - 10000$  MV; the temperature of thermal emission,  $T$ , sampled from  $5 \times 10^5 - 5 \times 10^8$  K and optical depth at  $1kT$ ,  $\tau_0$ , from  $0.01 - 1.0$  uniformly on a logarithmic scale; the current decay constant was taken as unit,  $a = 1$ ; the current rising constant  $a_1$  was sampled from  $0.01 - 0.7$ ; the voltage at the end of a discharge sampled from  $0.5V_0 - 5$  MV; the center of scattering angle region considered was taken randomly from  $0^\circ - 0.5^\circ$  and the width of the interval from  $0.1^\circ - 0.5^\circ$ . For each parameter set, we calculated the expected spectrum from the

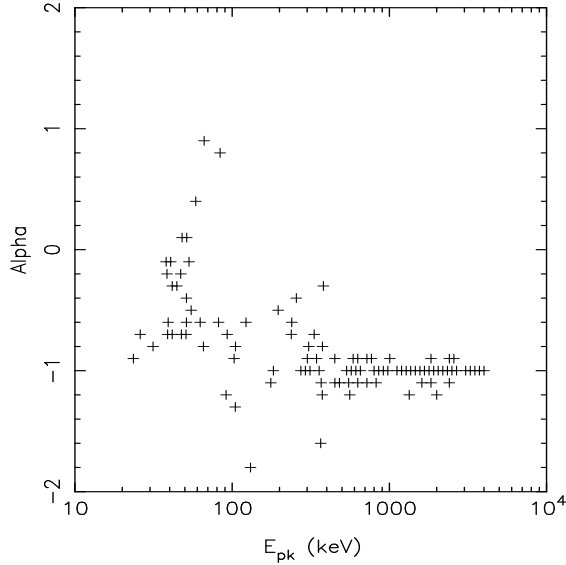


Figure 13: Distribution of  $\alpha$  and  $E_{pk}$  from the fit of Band *et al.* model to calculated spectra for 100 samples of discharge model.

discharge process and fitted the Band *et al.* model to. Most spectra fit well with the model, the average reduced  $\chi^2 = 1.2 \pm 0.3$ . Fig.13 is a plot of  $\alpha$  vs.  $E_{pk}$  from our calculations for 100 samples of discharge model, which shows a distribution quite similar with that from observed GRBs (see Preece *et al.* 1996, Fig.6). More calculations show that a summation of several spectra from different discharge columns with different parameters can also be well described by the Band *et al.* model.

A hard-to-soft spectral evolution has been observed for many bright GRBs (Ford *et al.* 1995; Briggs 1995): the peak energy,  $E_{pk}$ , softens over the burst. Liang & Kargatis (1996) further found that for a sample of bursts consisting of well resolved, isolated pulses  $E_{pk}$  decreases exponentially with photon fluence (running time integral of the flux), and that for many multi-pulse bursts, the exponential decay constant is invariant from pulse to pulse. The above properties can be interpreted easily in the frame of discharge mechanism. For example, we calculated time-resolved spectra for the discharge model described by Fig.12. To focus on the evolution of  $E_{pk}$ , we followed Liang & Kargatis (1996) to fix the two slopes throughout the burst by fitting the Band *et al.* model to the time-average spectrum Fig.12(b), the obtained time history of  $E_{pk}$ , Fig.14(a), shows a typical hard-to-soft evolution. In Fig.14(b)  $E_{pk}$  is plotted against photon fluence (the relative errors of  $E_{pk}$  are simply taken as 10%, a typical value for bright GRBs of BATSE), showing an exponential decay. It is found from calculations that the decay constant of  $E_{pk}$  versus fluence is mainly determined by the velocity of discharge voltage decaying, i.e. by the parameter  $B$  of discharge circuit. Therefore, the similarity of the exponential decay constants of the subsequent pulses to that of the leading pulse in samples of multi-pulse bursts can be explained as such pulses are from repeat discharges of the same circuit for the leading pulse. The softening trends in  $E_{pk}$  is not a universal property for the discharge model. For the case of both the initial discharge voltage and temperature being high, the cross section of Compton scattering falling with the increase of electron energy (Akhiezer & Berestetskii 1965) causes  $E_{pk}$  has not considerable change or even increase with time. Ford *et al.* (1995) have already observed such evolution trend in a few bursts. More dedicated model of discharge may explain the phenomenon of envelope decaying observed in long multi-pulse bursts (Ford *et al.* 1995).

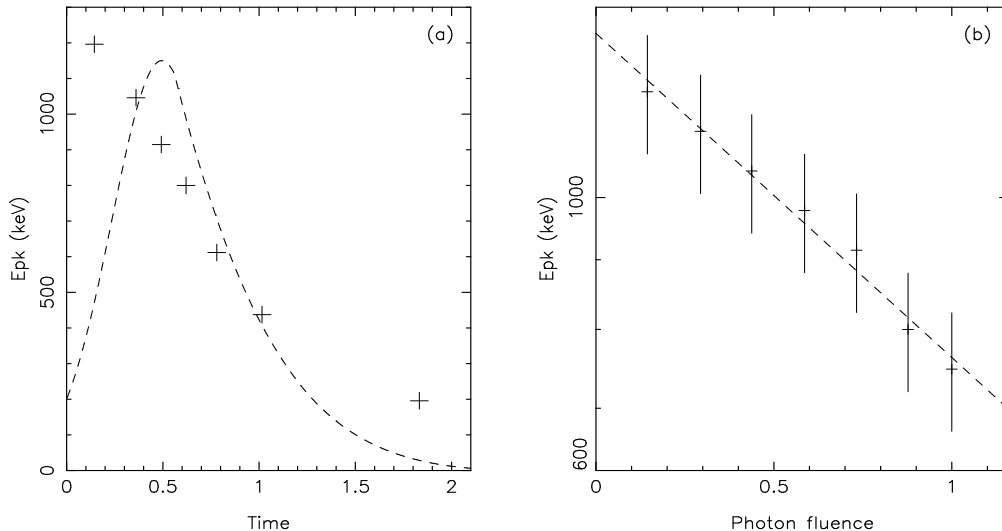


Figure 14: Spectral evolution expected for the discharge model described by Fig.12. (a) Time histories of  $E_{pk}$  (keV) (crosses) and photon flux (dashed line, in arbitrary units). The time is scaled by the decay time constant of discharging current. (b)  $E_{pk}$  versus photon fluence in units of total fluence. Relative errors of  $E_{pk}$  are taken as 10%. Dashed line shows an exponential decay.

Another natural deduction of the discharge model is the durations becoming shorter with increasing energy. For the discharge column described by Fig.12 we calculated the light curves in four energy channels: 20 – 50, 50 – 100, 100 – 300 and > 300 keV, and their autocorrelation functions respectively. The calculated autocorrelation function decreases more rapidly with time lag in the higher energy channels compared to the lowest one, as shown in Fig.15, which is consistent with that observed for GRBs (Link *et al.* 1993). We also calculated the cross-correlation functions between channel 1 (20 – 50 keV) and 3 (100 – 300 keV) and found a maximum at the time lag of  $-0.01$  (in units of the time constant  $a$  of current decay), indicating a time delay between soft and hard emissions, which is also observed in GRBs (Chipman 1993; Cheng *et al.* 1995).

#### 4. Discussion

The morphological diversity, the most striking feature of GRBs, is not a difficulty for the discharge mechanism to explain. Complicated patterns, such as wide variety of profile configurations, rich in fluctuation or smooth structures, rapid rise vs. slower fall, weak precursor and secondary pulses etc, are common in various electrical disruptive discharges, e.g. various kinds of gas discharge, high vacuum disruption, or lightning flashes. McBreen *et al.* (1994) have noted that there is considerable similarity in the statistical properties of the light curves and peak flux distributions of GRBs and terrestrial lightning: The range in durations of the flashes and multiple stroke patterns within the flashes are well fitted by lognormal distributions and the integral number versus peak flux distributions by truncated lognormal distributions. Fishman *et al.* (1994a) discovered a dozen of brief, intense gamma-ray flashes of atmospheric origin, terrestrial gamma-ray flashes (TGFs), from the first two years observation of BATSE. Although TGFs have durations, typically a few milliseconds, much shorter than GRBs, their time profiles showing complex features in wide variety are quite similar with GRBs. TGFs have hard spectra with the hardness ratio  $H_{32} = F_3/F_2$  being about two times  $\langle H_{32} \rangle$  for GRBs. For all bursts, of which the energy fluences  $F_2$  and  $F_3$  are available in the 3B catalog, we



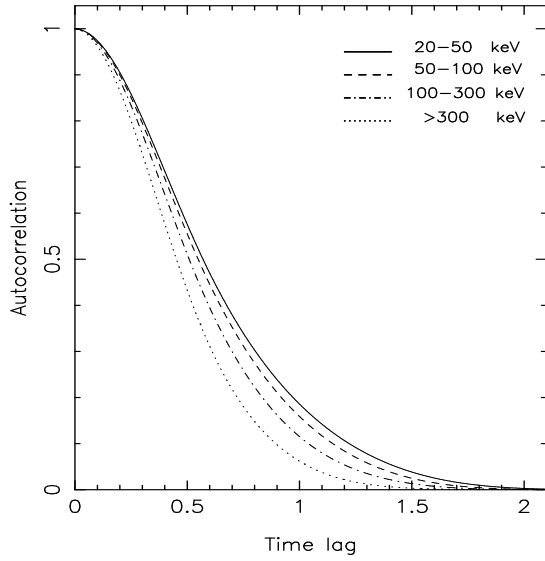


Figure 15: Autocorrelation functions of light curves in four energy channels expected by the discharge model of Fig.12 and Fig.14. The time lag is scaled by the time constant of discharging current decay.

found  $\langle H_{32} \rangle = 3.82$ . There exists an anti-correlation between GRB hardness and duration, hardness with short events in general being harder. Fig.16 shows the relation between the hardness ratio  $H_{32}$  and duration  $T_{90}$  in the 3B bursts and the regression line  $H_{32} = 5.1 - 1.1 \lg(T_{90}(s))$ . Extrapolating above relation to  $T_{90} = 5 \times 10^{-3}$  s, we expect  $H_{32} = 7.6$ , just about two times  $\langle H_{32} \rangle$ . Thus, besides the similarity in morphology, TGFs can be seen, in view of the spectral behaviour, as an extrapolation of GRBs. An evident correlation of TGFs with storm system indicates that these events are caused by electrical discharges to the stratosphere or ionosphere of the Earth (Fishman *et al.* 1994a), then TGFs give an observational evidence that the discharge process can produce high-energy bursts like GRBs.

Another kind of high-energy transients similar with GRBs is the solar hard X-ray flare. It is not easy to make the distinction between GRBs and solar hard X-ray flares just by their time profiles. In burst recognition, solar flares distinguished from GRBs by their locations near the sun, their generally soft spectra, and their coincidence with solar X-ray events detected by the GOES satellite (Fishman *et al.* 1994b). Opposite TGFs, solar flares are in general longer and softer than GRBs. From 1991 April 19 to 1995 November 28, there were a total of 4467 solar flares detected by BATSE, of which 677 gave rise to a burst trigger (SDAC 1996). Yu *et al.* (1997) have found that the intensity distribution of BATSE solar flares is very similar with that of GRBs. Fig.17 shows the intensity distribution of solar flares in the BATSE flare catalog and that of GRBs in the 3B catalog. The solar flare integral  $\lg N - \lg P$  distribution also appears a  $-3/2$  slope for bright events and saturated at low intensities like GRB does. After parallel translation the  $\lg N - \lg P$  diagram of solar flares is well coincidence with that of GRBs. This remarkable fact implies that the characteristic of GRB intensity distribution is not necessarily to be a measure of spatial homogeneity of burst sources, and that GRBs and solar flares may have similar production mechanism. Another noticed similarity between GRBs and solar flares is the delayed 1-GeV emission observed in both events (Kanbach *et al.* 1993; Hurley *et al.* 1994). In fact, Alfvén and Carlqvist (1967) suggested exploding discharges of electric double layers to be responsible for solar flares.

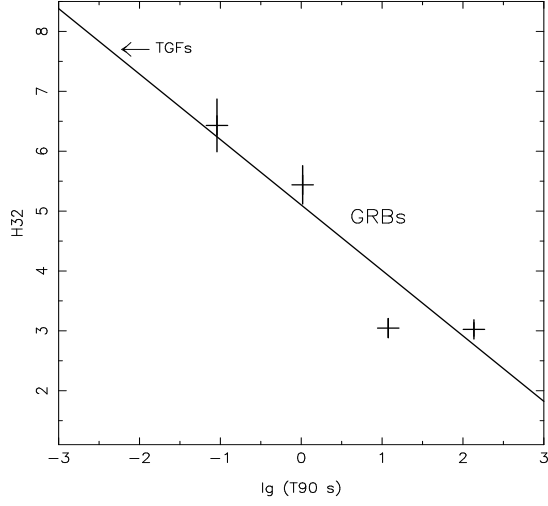


Figure 16: Correlation between hardness and duration of GRBs in 3B catalog. The arrow indicates the typical value of  $H_{32}$  for terrestrial  $\gamma$ -ray flashes detected by BATSE.

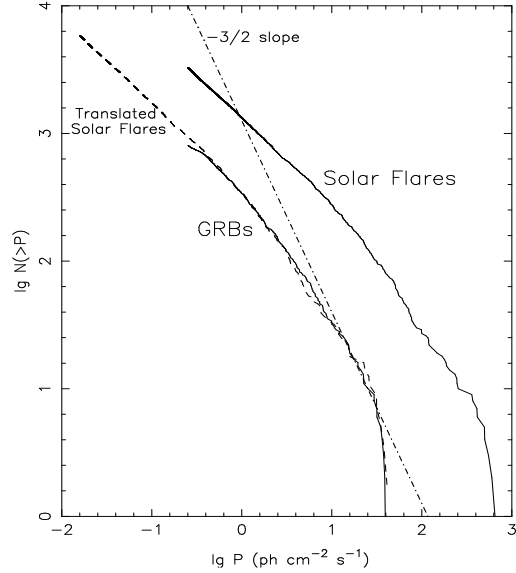


Figure 17: Integral intensity distributions of GRBs and solar flares. Peak fluxes  $P$  of GRBs are measured on the 1.024s timescale for 3B bursts, that of solar flares are taken from the BATSE solar flare catalog in SDAC for the period from 1991 April 19 to 1995 November 28. The dashed line is drawn from the solar flare  $\lg N - \lg P$  distribution by a parallel translation  $\lg N + 0.25, \lg P - 1.2$ .

*Acknowledgements.* This research has made of data obtained through the Compton Observatory Science Support Center and the Solar Data Analysis Center at the NASA-Goddard Space Flight Center. The author thanks Professors Lu Tan and Wu Mei for helpful discussions. This work was supported by the National Natural Science Foundation of China.

## References

- Akhiezer A.I. & Berestetskii V.B., 1965, Quantum Electrodynamics, John Wiley & Sons, Inc.
- Alfvén H., 1981, Cosmic Plasma, D.Reidel Publishing Company
- Alfvén H. and Carlqvist P., 1967, Solar Phys. 1, 220
- Band D.L. *et al.*, 1993, ApJ 413, 281
- Battan L.J., 1961, The Nature of Violent Storms, Doubleday, New York, 21
- Briggs M.S., 1995, in Ann. New York Acad. Sci.
- Cheng L.X., Ma Y.Q., Cheng K.S., Lu T. & Zhou Y.Y., 1995, A&A 300, 746
- Chipman E., 1993, in AIP Conf. Proc. 307: Gamma Ray bursts, Huntsville, p.202
- Dermer C.D., 1992, Phys. Rev. Letters 68, 1799
- Dezalay J.P. *et al.*, 1992, in AIP Conf. Proc.265, Gamma-Ray Bursts,
- Diaconis P. & Efron B., 1983, Scien. American, Sept. p.96
- Efron B. 1979, Ann. Statistics 7, 1
- Fishman G. J. *et al.*, 1989, in GRO science Workshop, Greenbelt, 2-39
- Fishman G.F. *et al.*, 1994a, Science 264, 1313
- Fishman G.F. *et al.*, 1994b, ApJS 92, 229
- Ford L.A. *et al.*, 1995, ApJ 439, 307
- Ginzburg V.L. & Syrovatskii S.I., 1964, The Origin of Cosmic Rays, Pergamon Press
- Hartmannm D.H., 1994, in G. Fishman, J. Brainerd & K. Hurley, eds. Gamma-Ray Bursts, 2nd Workshop, AIP Press, New York
- Hurley K. *et al.*, 1994, Nature 372, 652
- Kanbach G. *et al.*, 1993, A&AS 97, 349
- Klebesadel R., Strong I.B. and Olson R.A., 1973, ApJ 182, L85
- Kouveliotou C. *et al.*, 1993a, ApJ 413, L101
- Kouveliotou C. *et al.*, 1993b, A&AS 97, 55
- Krall N.E. & Trivelpiece A.W., 1973, Principles of Plasma Physics, McGraw-Hill, Inc.
- Kulsrud R.M., 1954, ApJ 119, 386
- Lamb D.Q., 1995, PASP 107, 1152
- Liang E. & Kargatis V., 1996, Nature 381, 49
- Li T.P., 1996, Chin. Phys. Lett. 13, 637
- Li T.P., 1997, Acta Astrophys. Sinica, in press

- Li T.P. & Wu M., 1997, Chin. Phys. Lett., in press
- Link B., Epstein R.I. & Priedhorsky W.C., 1993, ApJ 408, L81
- Mao S. & Paczyński B., 1992, ApJ 388, L45
- McBreen B., Hurley K.J., Long R. & Metcalfe L., 1994, MNRAS 271, 662
- Meegan C.A., Fishman G.J., Bhat N.D. *et al.*, 1996, The Third BATSE Gamma-Ray Burst Catalog, ApJS 106, 65
- Paczynski B., 1995, PASP 107, 1167
- Piran T., 1992, ApJ 389, L45
- Preece R. D. *et al.*, 1996, ApJ 473, 310
- SDAC, 1996, BATSE flare catalog, www address:  
[http://umbra.nascom.nasa.gov/batse/batse\\_years.html](http://umbra.nascom.nasa.gov/batse/batse_years.html)
- Sieger S., 1956, Nonparametric Statistics for The Behavioral Sciences, McGraw-Hill Book Comp., New York
- Suess S.T., 1990, Rev. Geophys., 28, 97
- Yu W.F., Li T.P., Wu M. & Song L.M., 1997, Acta Astrophys. Sinica, 17, 66